

Quasi-Newton FDE in One-Bit Pseudo-Randomly Quantized Massive MIMO-OFDM Systems

Gökhan Yılmaz, *Graduate Student Member, IEEE*, and Ali Özgür Yılmaz, *Member, IEEE*

Abstract—This letter offers a new frequency domain equalization (FDE) scheme that can work with a pseudo-random quantization (PRQ) scheme utilizing non-zero threshold quantization in one-bit uplink multi-user massive multiple-input multiple-output (MIMO) systems to mitigate quantization distortion and support high-order modulation schemes. The equalizer is based on Newton’s method (NM) and applicable for orthogonal frequency division multiplexing (OFDM) transmission under frequency-selective fading by exploiting the properties of massive MIMO. We develop a low-complexity FDE scheme to obtain a quasi-Newton method. The proposed detector outperforms the benchmark detector with comparable complexity.

Index Terms—Massive MIMO, OFDM, pseudo-random quantization (PRQ), one-bit ADC, FDE.

I. INTRODUCTION

MASSIVE multiple-input multiple-output (MIMO) systems are equipped with large numbers of base station (BS) antennas to achieve higher data rates in next-generation communication systems. However, cost and power consumption can be significant issues for these systems since each antenna requires a separate radio frequency (RF) chain. To remedy this problem, one-bit analog-to-digital converters (ADCs) have been proposed in [1]–[7]. However, the achievable rate is adversely affected due to the nonlinear distortion induced by the received signal. In particular, communication with high-order QAM constellations is difficult to achieve with one-bit ADCs due to the complete loss of amplitude information.

In our previous work [8], we aimed to tackle this issue by proposing new quantization and detection schemes for one-bit massive MIMO systems operating under frequency-flat fading. Inspired by the idea of randomizing the quantization operation to lower the quantization resolution in the temporal domain for general signal processing application from [9], we introduced a new pseudo-random quantization (PRQ) scheme by changing the domain of pseudo-randomization from temporal to spatial, in contrast to existing works such as [1]–[3], [6], [7], [10] where the quantization thresholds are taken to be zero for all receiver antennas. In [8], we show that by employing the PRQ approach, one-bit uplink massive MIMO systems can operate with higher rates and high-order QAM constellations such as 256-QAM or 1024-QAM provided that there is sufficient number of BS antennas by avoiding the performance degradation or saturation at high SNR stemming from the stochastic resonance with the conventional zero-threshold quantization (ZTQ) scheme.

G. Yılmaz (g.yilmaz@tue.nl) was and A. Ö. Yılmaz (aoyilmaz@metu.edu.tr) is with the Department of Electrical and Electronics Engineering, Middle East Technical University, Ankara, Turkey. G. Yılmaz is now with the Department of Electrical Engineering, Eindhoven University of Technology, Eindhoven, The Netherlands.

In this letter, we extend our previous work [8] to the frequency-selective fading scenario to analyze the effects of PRQ when there is inter-symbol interference (ISI) on the received signal in addition to multi-user interference (MUI). We formulate equalization in one-bit wideband massive MIMO systems as a constrained optimization problem and propose solving it using a second-order optimization technique, the projected Newton’s method (NM), applicable when a non-zero threshold quantization scheme is employed. Unlike [1], this approach does not require selecting suitable step sizes for different system setups due to the additional second-order derivative information. After deriving the necessary relations using NM, we utilize two approximations to decouple equalization among subcarriers and avoid matrix inversion to reach the proposed projected quasi-Newton detector (PQND), which is an essential improvement over [8], where the proposed time domain equalizer (TDE) under flat-fading would result in a substantial complexity increase under frequency-selective fading. In one-bit massive MIMO systems, adopting second-order optimization techniques to optimize the log-likelihood under frequency-selective fading has not been used. The proposed detector outperforms the benchmark detector from [1], irrespective of the quantization scheme.

II. SYSTEM MODEL

We consider an $N \times K$ uplink massive MIMO-OFDM system with V subcarriers, where K single-antenna users are served by a base station (BS) equipped with N antennas. We focus on a single-cell scenario and assume the analog frontend filters are sharp enough to avoid adjacent channel interference. Constellation symbols to be transmitted are selected independently from an M -QAM alphabet, denoted as $\bar{\mathcal{M}}$, with equal likelihood at all subcarriers and for all users. The frequency domain (FD) symbols of the users at the v^{th} subcarrier is shown as $\bar{\mathbf{x}}[v] = [\bar{x}_1[v] \ \bar{x}_2[v] \ \dots \ \bar{x}_K[v]]^T \in \mathbb{C}^K$ for $v = 0, 1, \dots, V-1$, where $\mathbb{E}[|\bar{x}_k[v]|^2] = E_s = 1$. The concatenated version of an FD vector for all subcarriers or a time domain (TD) vector for all time indices can be obtained as $\bar{\mathbf{x}} = [\bar{\mathbf{x}}[0]^T \ \bar{\mathbf{x}}[1]^T \ \dots \ \bar{\mathbf{x}}[V-1]^T]^T$. Each user transmits their FD symbols through inverse unitary discrete Fourier transform (DFT) before transmission to obtain their TD signals, which can be shown as $\bar{\mathbf{s}} = \mathbf{Q}_K^H \bar{\mathbf{x}} \in \mathbb{C}^{KV}$, where $\mathbf{Q}_i = \mathbf{F} \otimes \mathbf{I}_i$ for $i \in \mathbb{Z}^+$ and \mathbf{F} is the unitary DFT matrix of size $V \times V$. We assume the BS has perfect knowledge of the channel impulse response (CIR), and the multipath channel has L taps. Hence, each user adds a CP of length $L_{\text{CP}} \geq L-1$ to the beginning of their TD signals to help mitigate the effects of

ISI at the receiver side. The ℓ^{th} tap of CIR between all users and BS antennas can be represented as $\bar{\mathbf{H}}[\ell] \in \mathbb{C}^{N \times K}$, where the channel between the n^{th} BS antenna and the k^{th} user can be shown $\bar{h}_{n,k}[\ell]$. The CP is discarded at the receiver side. $\bar{\mathbf{y}}[m] = [\bar{y}_1[m] \ \bar{y}_2[m] \ \dots \ \bar{y}_N[m]]^T \in \mathbb{C}^N$ and $\bar{\mathbf{w}}[m] = [\bar{w}_1[m] \ \bar{w}_2[m] \ \dots \ \bar{w}_N[m]]^T \in \mathbb{C}^N$ represent the unquantized version of the received signal and the noise samples time m , respectively. $\bar{\mathbf{w}}[m] \sim \mathcal{CN}(\mathbf{0}_N, N_0 \mathbf{I}_N)$ for $m = 0, 1, \dots, V-1$, and there is no correlation among noise samples. We define the TD block circulant MIMO channel matrix of size $NV \times KV$ as

$$\begin{aligned} \bar{\mathbf{H}}_b &= \text{bcirc}\{\bar{\mathbf{H}}[0], \mathbf{0}, \dots, \mathbf{0}, \bar{\mathbf{H}}[L-1], \dots, \bar{\mathbf{H}}[1]\} \\ &= \bar{\mathbf{Q}}_N^H \bar{\mathbf{A}}_b \bar{\mathbf{Q}}_K, \end{aligned} \quad (1)$$

due to CP, where $\bar{\mathbf{A}}_b = \text{bdiag}\{\bar{\mathbf{A}}[0], \bar{\mathbf{A}}[1], \dots, \bar{\mathbf{A}}[V-1]\}$ is the block diagonal FD MIMO channel matrix. This decomposition utilizes the fact that the columns of the DFT matrix are eigenvectors of any circulant matrix and applies this to the MIMO scenario as in [11]. Hence, the unquantized representation of the received signal can be found using

$$\bar{\mathbf{y}} = \bar{\mathbf{H}}_b \bar{\mathbf{Q}}_K^H \bar{\mathbf{x}} + \bar{\mathbf{w}} = \bar{\mathbf{Q}}_N^H \bar{\mathbf{A}}_b \bar{\mathbf{x}} + \bar{\mathbf{w}} = \bar{\mathbf{G}} \bar{\mathbf{x}} + \bar{\mathbf{w}}, \quad (2)$$

where $\bar{\mathbf{G}} = \bar{\mathbf{Q}}_N^H \bar{\mathbf{A}}_b$ represents the effective TD channel matrix, $\bar{\mathbf{w}}$ is the spatially and temporally white thermal noise vector. Then, the unquantized representation of the observations can be used to find the one-bit quantized observations as

$$\bar{\mathbf{r}} = \text{sign}(\Re\{\bar{\mathbf{y}} - \bar{\boldsymbol{\tau}}\}) + j \text{sign}(\Im\{\bar{\mathbf{y}} - \bar{\boldsymbol{\tau}}\}), \quad (3)$$

where $\bar{\boldsymbol{\tau}}$ is the time-invariant quantization threshold vector with components $\bar{\boldsymbol{\tau}}[m_1] = \bar{\boldsymbol{\tau}}[m_2] = \bar{\boldsymbol{\tau}}$ for $m_1, m_2 \in \{0, 1, \dots, V-1\}$. These thresholds need not be updated for different channel realizations. The detailed procedure regarding pseudo-random threshold assignment is explained in Section IV. Due to the structure of the proposed detector, we need to be able to work with real numbers only. The relation between a complex vector $\bar{\mathbf{a}}$ and its real counterpart \mathbf{a} , and a complex matrix $\bar{\mathbf{A}}$ and its real counterpart \mathbf{A} can be obtained as

$$\mathbf{a} = \begin{bmatrix} \Re\{\bar{\mathbf{a}}\} \\ \Im\{\bar{\mathbf{a}}\} \end{bmatrix}, \text{ and } \mathbf{A} = \begin{bmatrix} \Re\{\bar{\mathbf{A}}\} & -\Im\{\bar{\mathbf{A}}\} \\ \Im\{\bar{\mathbf{A}}\} & \Re\{\bar{\mathbf{A}}\} \end{bmatrix}, \quad (4)$$

respectively. (3) can be re-written as $\mathbf{r} = \text{sign}(\mathbf{G} \mathbf{x} - \boldsymbol{\tau} + \mathbf{w})$. We define the signal-to-noise ratio (SNR) as the ratio of the average received signal power per user to the average noise power at each antenna such that $\rho = E_s/N_0 = 1/N_0$.

III. PROJECTED QUASI-NEWTON DETECTOR (PQND)

In the presence of independent additive white Gaussian noise (AWGN) on each branch of a one-bit quantized channel, as in [1], [4], [12], the log-likelihood can be expressed as

$$\mathcal{L}(\mathbf{x}) = \mathbf{1}_{2NV}^T \log \left(\Phi \left(\sqrt{\frac{2}{N_0}} \mathbf{r} \odot (\mathbf{G} \mathbf{x} - \boldsymbol{\tau}) \right) \right), \quad (5)$$

where $\Phi(x) = \int_{-\infty}^x \phi(\tau) d\tau$ is the cumulative distribution function (CDF) of the standard Gaussian random variable with

$\phi(x) = \frac{\exp(-x^2)}{\sqrt{2\pi}}$, and $\mathbf{1}_i$ is the vector of size $i \in \mathbb{Z}^+$, whose elements are all set to 1. $\log(\cdot)$ and $\Phi(\cdot)$ are applied element-wise on their arguments. The optimal solution to this problem requires an exhaustive search of all possible candidates from a discrete set. Subcarrier-level ML detection in the FD is not applicable since conversion to the FD causes an unknown conditional distribution for the quantized observations due to quantization noise. As in [1], in order to utilize gradient-based optimization techniques, we relax the discrete input set constraint in maximum likelihood sequence detection (MLSD) and reformulate the problem as

$$\begin{aligned} \tilde{\mathbf{x}} &= \arg \max_{\mathbf{x} \in \mathbb{R}^{2KV}} \mathcal{L}(\mathbf{x}) \\ &\text{subject to } |\tilde{x}_i| \leq M_b, \quad i = 1, 2, \dots, 2KV, \end{aligned} \quad (6)$$

where M_b is the boundary of the chosen constellation in one of the I/Q parts. Due to the log-concavity of $\Phi(\cdot)$, we have a concave optimization problem, which can be solved with gradient-based optimization methods [1], [4], [12]. The convergence of concave optimization problems of similar forms is shown in [13]. While relaxing the discrete input set constraint, we utilize a restriction. Each element of \mathbf{x} is inside the boundaries of the constellation, which is called the box constraint [1]. Also, once a solution to this problem is obtained, the norm of \mathbf{x} is set to KV , which is called the norm projection as in [12].¹ The box constraint prevents diverging from the constellation's boundaries during equalization, using a priori knowledge of the chosen constellation scheme. To apply constrained optimization, we resort to the projection method. We start with projected NM, a second-order optimization technique, to solve (6). The update equation can be written as

$$\mathbf{x}^{(t)} = \mathcal{P}^{(t)} \left(\mathbf{x}^{(t-1)} - \alpha (\nabla^2 \mathcal{L}^{(t-1)})^{-1} \nabla \mathcal{L}^{(t-1)} \right), \quad (7)$$

where $\alpha \in \mathbb{R}$ is the step size, and $\mathcal{P}^{(t)}(\cdot)$ is the projection function at iteration t , which can be expressed as

$$\mathcal{P}^{(t)}(\tilde{\mathbf{x}}) = \begin{cases} \mathcal{P}_{\text{box}}(\tilde{\mathbf{x}}), & 1 \leq t < T \\ \mathcal{P}_{\text{norm}}(\tilde{\mathbf{x}}), & t = T, \end{cases} \quad (8)$$

where T denotes the total number of iterations. $\mathcal{P}_{\text{box}}(\tilde{\mathbf{x}}) = \mathcal{P}_{\text{box}}^I(\Re\{\tilde{\mathbf{x}}\}) + j \mathcal{P}_{\text{box}}^Q(\Im\{\tilde{\mathbf{x}}\})$, where $\mathcal{P}_{\text{box}}^I(\cdot) = \mathcal{P}_{\text{box}}^Q(\cdot)$ and it is defined as $\mathcal{P}_{\text{box}}^I(x) = \text{sign}(x) \min\{|x|, M_b\}$, and each function is applied element-wise on its arguments. We define the norm projection function as $\mathcal{P}_{\text{norm}}(\tilde{\mathbf{x}}) = \frac{\sqrt{KV}}{\|\tilde{\mathbf{x}}\|} \tilde{\mathbf{x}}$. As in [12], norm projection is applied only at the last iteration. In (7), $\nabla \mathcal{L}^{(t)}$ is the gradient of the log-likelihood function \mathcal{L} with respect to \mathbf{x} calculated at iteration t . Similarly, $\nabla^2 \mathcal{L}^{(t)}$ is the Hessian of \mathcal{L} with respect to \mathbf{x} at iteration t . The gradient and Hessian are functions of \mathbf{x} , and we drop the argument for ease of notation. Also, we define a new vector $\mathbf{u} = \sqrt{\frac{2}{N_0}} \mathbf{r} \odot (\mathbf{G} \mathbf{x} - \boldsymbol{\tau})$ for compactness. The gradient can be found as

$$\nabla \mathcal{L} = \sqrt{\frac{2}{N_0}} \mathbf{G}^T (\mathbf{r} \odot \varphi(\mathbf{u})), \quad (9)$$

¹The norm projection is related to the law of large numbers (LLN) for which we can utilize practical values of V being large.

where $\varphi(x) \triangleq \frac{d}{dx} \ln(\Phi(x)) = \phi(x)/\Phi(x)$, and it is applied element-wise on its arguments. Notice that, $\varphi(x) \geq 0$ for all $x \in \mathbb{R}$. The Hessian matrix can be found as

$$\nabla^2 \mathcal{L} = \frac{2}{N_0} \underline{\mathbf{G}}^T \text{diag}(\psi(\underline{\mathbf{u}})) \underline{\mathbf{G}}, \quad (10)$$

where $\psi(x) \triangleq \frac{d^2}{dx^2} \ln(\Phi(x)) = -x\varphi(x) - \varphi^2(x)$, and it is applied element-wise on its arguments. Note that $\psi(x) \leq 0$ for all $x \in \mathbb{R}$, which shows the log-concavity of $\Phi(\cdot)$. The computations of these nonlinear functions in finite precision can cause divergent behavior for which the solution in [8, Appendix B] is also used herein. NM can provide complexity reduction. However, it does not allow subcarrier-level equalization and requires a large matrix inversion. We attempt to solve these problems using approximations to obtain an equalization method with lower complexity. We define the step $\Delta \underline{\mathbf{x}} = (\nabla^2 \mathcal{L})^{-1} \nabla \mathcal{L}$ which can be written as

$$\Delta \underline{\mathbf{x}} = \sqrt{\frac{N_0}{2}} \left(\underline{\mathbf{G}}^T \text{diag}(\psi(\underline{\mathbf{u}})) \underline{\mathbf{G}} \right)^{-1} \left(\underline{\mathbf{G}}^T (\underline{\mathbf{r}} \odot \varphi(\underline{\mathbf{u}})) \right). \quad (11)$$

The Hessian matrix $\underline{\mathbf{A}}_b^T \mathbf{Q}_N \text{diag}(\psi(\underline{\mathbf{u}})) \mathbf{Q}_N^T \underline{\mathbf{A}}_b$ to be inverted is a $2KV \times 2KV$ matrix. In order to simplify the relations, we first aim to approximate $\text{diag}(\psi(\underline{\mathbf{u}}))$ to a multiple of the identity matrix $\gamma \mathbf{I}_{2NV}$ such that $\gamma = \frac{1}{2NV} \sum_{n=1}^{2NV} \psi(\underline{\mathbf{u}}_n)$. This approximation is valid for the low SNR regime when N_0 is large so that the elements of $\underline{\mathbf{u}}$ are very close to zero. For the high SNR regime, it is very likely that all elements of $\underline{\mathbf{u}}$ are positive and large values. Since the rate of change of $\psi(\cdot)$ is very low for large positive arguments, this approximation is also helpful for high SNR. Massive MIMO helps obtain an accurate approximation of the mean for both regimes. Note that with this approximation, decoupling between the real and imaginary parts due to second-order derivative calculation can also be avoided. We can now go back to the notation with complex numbers. The complex counterpart of (7) for the quasi-Newton approach can be obtained as $\bar{\underline{\mathbf{x}}}^{(t)} = \mathcal{P}^{(t)}(\bar{\underline{\mathbf{x}}}^{(t-1)} - \alpha \Delta \bar{\underline{\mathbf{x}}}^{(t-1)})$, where $\Delta \bar{\underline{\mathbf{x}}}$ can be written as

$$\Delta \bar{\underline{\mathbf{x}}} \cong \frac{1}{\gamma} \sqrt{\frac{N_0}{2}} \left(\underline{\mathbf{A}}_b^H \underline{\mathbf{A}}_b \right)^{-1} \underline{\mathbf{A}}_b^H \bar{\mathbf{Q}}_N (\bar{\underline{\mathbf{r}}} \odot \bar{\varphi}(\bar{\underline{\mathbf{u}}}), \quad (12)$$

by defining $\bar{\varphi}(\bar{\mathbf{a}}) = \varphi(\Re\{\bar{\mathbf{a}}\}) + j\varphi(\Im\{\bar{\mathbf{a}}\})$ and \odot product of two vectors $\bar{\mathbf{a}}$ and $\bar{\mathbf{b}}$ as $\bar{\mathbf{a}} \odot \bar{\mathbf{b}} = \Re\{\bar{\mathbf{a}}\} \odot \Re\{\bar{\mathbf{b}}\} + j \Im\{\bar{\mathbf{a}}\} \odot \Im\{\bar{\mathbf{b}}\}$. Note that $\bar{\underline{\mathbf{u}}}$ from its each component $\{\bar{\underline{\mathbf{u}}}[m]\}_{m=0}^{V-1}$ can be found with the complex notation as

$$\bar{\underline{\mathbf{u}}}[m] = \sqrt{\frac{2}{N_0}} \bar{\mathbf{r}}[m] \odot (\mathcal{F}_m^{-1}\{\bar{\mathbf{A}}[v]\bar{\underline{\mathbf{x}}}[v]\} - \bar{\tau}), \quad (13)$$

where $\mathcal{F}_m^{-1}(\cdot) = \sum_{v=0}^{V-1} (\cdot) \exp(j2\pi \frac{mv}{V})$. Since $\underline{\mathbf{A}}_b$ is a block diagonal matrix, subcarrier-level processing is now applicable. (12) can be written for each subcarrier $v = 0, 1, \dots, V-1$ as

$$\Delta \bar{\underline{\mathbf{x}}}[v] \cong \frac{1}{\gamma} \sqrt{\frac{N_0}{2}} \bar{\mathbf{A}}[v]^\dagger \mathcal{F}_v \{\bar{\mathbf{r}}[m] \odot \bar{\varphi}(\bar{\underline{\mathbf{u}}}[m])\}. \quad (14)$$

where $\mathcal{F}_v(\cdot) = \sum_{m=0}^{V-1} (\cdot) \exp(-j2\pi \frac{mv}{V})$ and $\bar{\mathbf{A}}[v]^\dagger =$

$(\bar{\mathbf{A}}[v]^H \bar{\mathbf{A}}[v])^{-1} \bar{\mathbf{A}}[v]^H$. In order to avoid matrix inversion, we introduce one last approximation using the properties of massive MIMO systems. Notice that $\bar{\mathbf{A}}[v]^\dagger$ from (14) is the zero-forcing (ZF) filter. By exploiting the large N , we assume $\bar{\mathbf{A}}[v]^H \bar{\mathbf{A}}[v]$ is diagonally-dominant, and $(\bar{\mathbf{A}}[v]^H \bar{\mathbf{A}}[v])^{-1}$ can be approximated by only its diagonal part as $\boldsymbol{\lambda}[v]$ such that $\lambda_k[v] = 1/\sum_{n=1}^N |[\bar{\mathbf{A}}[v]]_{(n,k)}|^2$ for $k = 1, 2, \dots, K$ and $v = 0, 1, \dots, V-1$. Hence, we replace the ZF filter expression during the step calculations with the maximum ratio combining (MRC) filter by relying on massive MIMO, i.e., $N \gg K$, to obtain the final form

$$\Delta \bar{\underline{\mathbf{x}}}[v] \cong \frac{1}{\gamma} \sqrt{\frac{N_0}{2}} \boldsymbol{\lambda}[v] \odot (\bar{\mathbf{A}}[v]^H \mathcal{F}_v \{\bar{\mathbf{r}}[m] \odot \bar{\varphi}(\bar{\underline{\mathbf{u}}}[m])\}). \quad (15)$$

Before starting the iterative updates, an initial solution should be found, preferably not far from the optimum. The MRC estimate is a suitable choice with its low complexity, which can be found as $\bar{\underline{\mathbf{x}}}^{(0)}[v] = \sqrt{\frac{\pi\sigma_y^2}{4}} \boldsymbol{\lambda}[v] \odot (\bar{\mathbf{A}}[v]^H \mathcal{F}_v \{\bar{\mathbf{r}}[m]\})$ for $v = 0, 1, \dots, V-1$, where $\sigma_y^2 = K + N_0 + \sigma_\tau^2$ and σ_τ^2 is the variance of the quantization thresholds.² At high SNR, to avoid singular Hessian matrices, we define a damping factor as in [8] such that $\zeta = \max\{1, \rho/\rho_d\}$, where ρ_d is the damping SNR, and the actual N_0 is multiplied with ζ . After the iterative updates, symbol-by-symbol minimum distance mapping is applied to the estimate.

IV. PSEUDO-RANDOM QUANTIZATION (PRQ) SCHEME

Each pair of ADCs in the BS RF chains has a complex-valued threshold that separately represents the I/Q parts. The thresholds are generated from the Gaussian distribution, i.e., $\bar{\tau} \sim \mathcal{CN}(\mathbf{0}_N, \sigma_\tau^2 \mathbf{I}_N)$ as in the conventional dithering scenario. In [8], we parameterize the variance of the thresholds using empirical observations for flat-fading channels, which depend on the system parameters. As in [8], the threshold SNR value above which PRQ is utilized is determined as

$$\rho_t = 0.15K^2 + L_s - 2.50 \log_2(N) + 14 \text{ dB} \quad (16)$$

where L_s is the number of strong, i.e., high-power channel taps, which is determined by checking the numbers of taps with an average power stronger than that of a uniform power delay profile (PDP) channel with the same delay spread. The only difference compared to [8] is the channel's frequency-selectivity, for which the channel's delay spread is considered. As in [8], the variance of the quantization thresholds is found accordingly using $\sigma_\tau^2 = \mathbf{R}(E_s/\rho_t - N_0) = \mathbf{R}(1/\rho_t - N_0)$, where $\mathbf{R}(x) = \max\{0, x\}$ is the unit ramp function. Hence, the threshold variance is gradually increased above the threshold SNR value.

V. COMPUTATIONAL COMPLEXITY ANALYSIS

Since $N \gg K$ for massive MIMO, the complexity-dominant parts of the algorithm are computations of $\bar{\underline{\mathbf{u}}}$ and $\Delta \bar{\underline{\mathbf{x}}}$ both with

² $\bar{\tau}$ acts as an additional form of AWGN by taking the quantization thresholds to be random. The scaling factor $\sqrt{\pi\sigma_y^2/4}$ is added to compensate for the missing quantization label for linear processing as in [8], which is obtained using the Bussgang decomposition and assuming an effective diagonal covariance matrix $\sigma_y^2 \mathbf{I}_{NV}$ for $\bar{\underline{\mathbf{y}}}$.

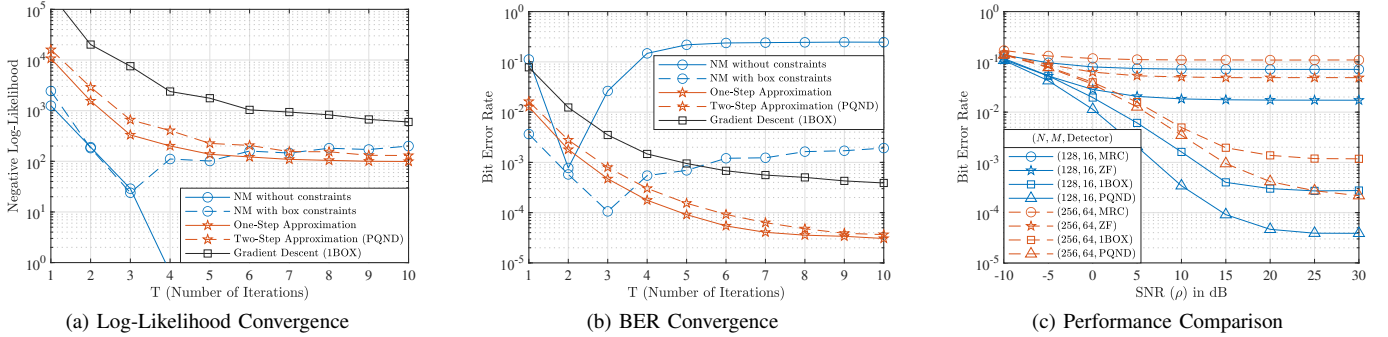


Fig. 1. (a)-(b) Convergence analysis of the methods in terms of the negative of the log-likelihood and BER analysis in a 128×10 system with $V = 32$, employing ZTQ and 16-QAM constellation in the SDS channel. $\alpha = 1, 0.8, 0.7, 0.009$ for NM, its one and two-stage approximated versions, 1BOX, respectively. (c) Comparison of the BER performances of MRC, ZF, 1BOX [1], and PQND methods with ZTQ in the LDS channel with respect to SNR.

TABLE I
COMPLEXITY COMPARISON OF PQND WITH EXISTING METHODS

Detector	Number of Flops
GEC-SR [3]	$\mathcal{O}(TNV \log_2(NV)) + \mathcal{O}(TN^2V)$
EM and GAMP [6]	$\mathcal{O}(TNKV^2)$
PQND, 1BOX [1], and IEM [7]	$\mathcal{O}(TVN \log_2(V)) + \mathcal{O}(TVNK)$
NM	$\mathcal{O}(TVNK^2V^3)$

complexity $\mathcal{O}(TVN \log_2(V)) + \mathcal{O}(TVNK)$. The complexities of the proposed detector and the existing works from the literature are shown in Table I. The generalized expectation consistent signal recovery (GEC-SR) method [3] requires a quadratic complexity increase in the number of BS antennas. EM and GAMP methods, explained in detail in [6], require a quadratic complexity increase in the data block length. Inexact EM (IEM) [7] and 1BOX [1] methods have comparable complexity with the proposed PQND method. However, the performance of the IEM method is very similar to 1BOX, and the number of iterations for the algorithm to converge is very large [7]. The benchmark algorithm to compare with the proposed PQND is the 1BOX detector from [1], which utilizes FDE tools with first-order optimization.

VI. SIMULATION RESULTS

In this section, the error performance of the proposed detector is investigated. PQND's step size is $\alpha = 0.7$ for all scenarios. $T = 6$ iterations are considered for all scenarios. The damping SNR for PQND is determined as $\rho_d = 20 - 150 \frac{K}{N}$ dB. The number of subcarriers is chosen as $V = 256$ unless otherwise stated. The wireless channel is modeled as Rayleigh fading, i.e., $\bar{h}_{n,k}[\ell] \sim \mathcal{CN}(0, p[\ell])$, and each coefficient is statistically independent both in space and time. The uncoded BER performance is investigated with two PDPs. The power of each tap in an exponential PDP channel can be calculated as $p[\ell] = \frac{\exp(-\mu\ell)}{\sum_{m=0}^{L-1} \exp(-\mu m)}$ where μ is the power decay rate. To model a small delay spread (SDS) channel, we use exponential PDP where $L = 8$ and $\mu = 1$, which results in $L_s = 3$. To model a large delay spread (LDS) channel, we utilize TDL-A delay profile from [14], which is a tapped delay line channel model introduced by 3GPP, for which $L = 23$ and $L_s = 7$.

An empirical convergence analysis is shown in Fig. 1a and 1b. The initial solution is used as the MRC estimate for all

algorithms, and the same projection functions are applied for all methods for fairness. If NM is used with approximations, it can easily be seen that we can obtain convergence. Also, the PQND method performs very closely to the one-step approximated method, which is a rational trade-off to avoid matrix inversion. Even after careful adjustments of the step size for the 1BOX method, it fails to converge within 10 iterations. Note that even though NM without constraints converges quickly in the log-likelihood sense, it does converge to the optimal solution since the input comes from a discrete alphabet. Also, the original NM with box constraints fails to converge after hitting a minimum, but PQND does not face such problems.

The BER performances of different detectors from the literature are compared in Fig. 1c in the LDS channel with ZTQ. The ZF estimate can be found as $\tilde{\mathbf{x}}[v] = \sqrt{\frac{\pi\sigma_y^2}{4}} \bar{\mathbf{A}}[v]^\dagger \mathcal{F}_v \{\bar{\mathbf{r}}[m]\}$. 1BOX involves only box projections at each iteration, though for fairness during comparison, we utilize the same projection function for 1BOX as PQND. Regarding the damping constant, a similar discussion about acting as if the SNR is lower than its actual value is made in [1]. From several trials, we have seen that choosing $\rho_d = 15$ dB for 1BOX is suitable for both system setups. $T = 6$ iterations of 1BOX are utilized, the same as PQND. The step size is an issue for first-order optimization methods, especially for varying SNR. We select the step size of 1BOX as 0.007. Linear detectors MRC and ZF perform much poorly compared to the more sophisticated methods 1BOX and PQND. For a fixed T , the proposed PQND outperforms 1BOX in all scenarios since second-order techniques converge faster.

In Fig. 2a, the system's performance is investigated when ZTQ and PRQ schemes are utilized with high-order modulations in the SDS channel using PQND and 1BOX.³ The high SNR performance generally starts to saturate with ZTQ after some point. The spatial degrees of freedom are exploited much better with PRQ, and high SNR error floors are decreased to much lower levels. Existing methods for one-bit massive MIMO focus on QPSK and 16-QAM constellations. According to the results, higher-order modulation schemes can also be applicable in one-bit massive MIMO systems with the PRQ scheme. PQND and 1BOX perform similarly with PRQ for

³We modify 1BOX for PRQ by updating the log-likelihood function according to the quantization thresholds.

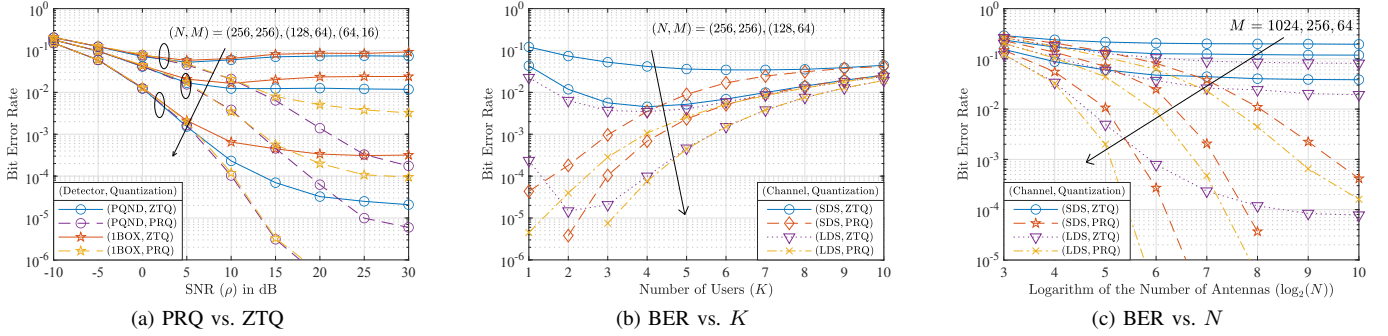


Fig. 2. (a) The performance comparison of PQND and 1BOX [1] with respect to SNR in the SDS channel using ZTQ and PRQ where $K = 2$. With 1BOX, $\alpha = 0.02, 0.01, 0.007$ for $N = 64, 128, 256$, respectively. (b) The BER performance against K at $\rho = 30$ dB with ZTQ and PRQ in the SDS and LDS channels. (c) The BER performance against $\log_2(N)$ when $K = 1$ at $\rho = 30$ dB with ZTQ and PRQ in the SDS and LDS channels.

16-QAM, yet PQND is significantly better at higher M .

In Fig. 2b, the PQND performances in the SDS channel with respect to K are plotted using ZTQ and PRQ. Since the high SNR performance is the limiting factor, $\rho = 30$ dB is selected. Similar to the findings from [8], starting with the single-user scenario, increasing K results in better performance at the beginning, which are implications of the SR phenomenon and MUI serving as a source of dither. The performance gain obtained with PRQ is more significant for relatively small K values. The LDS channel exhibits a higher ISI level than the SDS channel, which leads to better performance. Starting with $K = 1$, K for which ZTQ and PRQ start to perform the same is smaller for the LDS channel. These results suggest that at high SNR, up to a certain point of sum interference composed of MUI and ISI, massive MIMO systems can benefit from PRQ to achieve higher rates per user by employing higher M . In Fig. 2c, we obtain the PQND performances when $K = 1$ with respect to $\log_2(N)$ at $\rho = 30$ dB both in SDS and LDS channels. The SDS channel does not allow the usage of these high-order modulation schemes with the conventional ZTQ, even when N is very large. Hence, in the single-input multiple-output SIMO scenario with no MUI, ISI helps lower the amplitude distortion as suggested in [5]. However, even in the LDS channel, utilizing PRQ is necessary to work with 256-QAM and 1024-QAM.

VII. CONCLUSION

This letter proposes a new detection method called PQND that operates with PRQ for one-bit massive MIMO-OFDM systems. PQND is derived based on NM with additional approximations to obtain a quasi-Newton method by operating at the subcarrier level in the FD. By utilizing PQND and PRQ, one-bit massive MIMO-OFDM systems can support high-order modulation schemes and benefit from higher rates per user at high SNR, especially for less dispersive channels, e.g., mmWave channel. The proposed detector outperforms the benchmark method 1BOX with comparable complexity.

ACKNOWLEDGMENTS

The work of G. Yılmaz was supported by Vodafone Turkey within the framework of the 5G and Beyond Joint Graduate

Support Program coordinated by the Information and Communication Technologies Authority of Turkey.

REFERENCES

- [1] S. H. Mirfarshbafan, M. Shabany, S. A. Nezamathosseini, and C. Studer, "Algorithm and VLSI design for 1-bit data detection in massive MIMO-OFDM," *IEEE Open J. of Circuits and Syst.*, vol. 1, pp. 170–184, 2020.
- [2] Ö. T. Demir and E. Björnson, "ADMM-based one-bit quantized signal detection for massive MIMO systems with hardware impairments," in *ICASSP 2020 IEEE Int. Conf. Acoust., Speech and Signal Process.*, 2020, pp. 9120–9124.
- [3] H. He, C.-K. Wen, and S. Jin, "Bayesian optimal data detector for hybrid mmWave MIMO-OFDM systems with low-resolution ADCs," *IEEE J. Sel. Top. in Signal Process.*, vol. 12, no. 3, pp. 469–483, 2018.
- [4] J. Choi, J. Mo, and R. W. Heath, "Near maximum-likelihood detector and channel estimator for uplink multiuser massive MIMO systems with one-bit ADCs," *IEEE Trans. Commun.*, vol. 64, no. 5, pp. 2005–2018, 2016.
- [5] C. Mollén, J. Choi, E. G. Larsson, and R. W. Heath, "Uplink performance of wideband massive MIMO with one-bit ADCs," *IEEE Trans. Wirel. Commun.*, vol. 16, no. 1, pp. 87–100, 2017.
- [6] J. García, J. Munir, K. Roth, and J. A. Nossek, "Channel estimation and data equalization in frequency-selective MIMO systems with one-bit quantization," *CoRR*, vol. abs/1609.04536, 2016. [Online]. Available: <http://arxiv.org/abs/1609.04536>
- [7] M. Shao and W.-K. Ma, "Divide and conquer: One-bit MIMO-OFDM detection by inexact expectation maximization," in *ICASSP 2021 IEEE Int. Conf. Acoust., Speech and Signal Process.*, 2021, pp. 4890–4894.
- [8] G. Yılmaz and A. Ö. Yılmaz, "Pseudo-random quantization based two-stage detection in one-bit massive MIMO systems," 2023, submitted to *IEEE Trans. Wirel. Commun.* and it is currently under review. [Online]. Available: <https://arxiv.org/abs/2306.04329>
- [9] I. Bilinskis, "Pseudo-randomized quantizing," in *Digital Alias-Free Signal Processing*. USA: John Wiley & Sons, Inc., 2007, pp. 107–126.
- [10] A. B. Üçüncü and A. Ö. Yılmaz, "Oversampling in one-bit quantized massive MIMO systems and performance analysis," *IEEE Trans. Wirel. Commun.*, vol. 17, no. 12, pp. 7952–7964, 2018.
- [11] A. B. Üçüncü, E. Björnson, H. Johansson, A. Ö. Yılmaz, and E. G. Larsson, "Performance analysis of quantized uplink massive MIMO-OFDM with oversampling under adjacent channel interference," *IEEE Trans. Commun.*, vol. 68, no. 2, pp. 871–886, 2020.
- [12] L. V. Nguyen, A. L. Swindlehurst, and D. H. N. Nguyen, "Linear and deep neural network-based receivers for massive MIMO systems with one-bit ADCs," *IEEE Trans. Wirel. Commun.*, vol. 20, no. 11, pp. 7333–7345, 2021.
- [13] J. Choi, D. J. Love, D. R. Brown, and M. Boutin, "Quantized distributed reception for MIMO wireless systems using spatial multiplexing," *IEEE Trans. Signal Process.*, vol. 63, no. 13, pp. 3537–3548, 2015.
- [14] 3rd Generation Partnership Project (3GPP), "Study on channel model for frequencies from 0.5 to 100 GHz," Technical Report (TR) 38.901, 11 2020, version 16.1.0. [Online]. Available: https://www.etsi.org/deliver/etsi_tr/138900_138999/138901/16.01.00_60/tr_138901v160100p.pdf